Simulation of gravity driven free-surface flow in fractured geological media

Jannes Kordilla, Tobias Geyer
Applied Geosciences
Georg-August-Universität Göttingen
Göttingen, Germany
jkordil@gwdg.de

Alexandre Tartakovsky
Computational Science and Mathematics Division
Pacific Northwest National Laboratory
Richland, USA
alexandre.tartakovsky@pnnl.gov

***Abstract*—Simulation of unsaturated free-surface flow in fractured geological media represents a challenge due to the highly heterogeneous flow field induced by extensive faults, joints and fissures. Free-surface flow in unsaturated media leads to highly intermittent flow regimes and flow velocities well above those assumed for the bulk volume. However, common modeling approaches relying on volume-averaged effective equations fail to capture this flow feature. In this work we present micro-scale flow simulations using a three-dimensional multiphase SPH code. Pairwise fluid-fluid and solid-fluid interaction forces are used to simulate a wide range of wetting conditions encountered on rock surfaces. It is shown that static contact angles for sessiles droplets are independent of the model discretization, i.e. the total amount of particles. Thus, computation times can be reduced without sacrificing qualitative or quantitative information. Furthermore we show that our model is in accordance with general scaling laws for droplet flow.**

I. Introduction

Facing a global climate change and a rapidly growing world population the management of limited water resources becomes increasingly difficult. Aquifers (i.e. porous and/or fractured rocks from which economically profitable quantities of water can be extracted) provide the main storage for fresh water within the hydrogeological cycle between atmosphere and surface waters. The subsurface can be divided into (1) an unsaturated and (2) a saturated zone. The saturated zone is delineated by the water table, i.e. all available voids are filled with water, whereas the unsaturated zone comprises the part of the subsurface between water table and surface where pores and fractures are only partially filled with water. The unsaturated zone therefor provides the main pathway for precipitation and surface waters to the saturated zone.

Compared to unconsolidated porous media tectonically stressed aquifers provide additional highly conductive fractures, joints and faults embedded in a low conductive matrix. Even though their total fraction of the aquifers porosity may be as low as $1\,\%$ [1] the importance of fractures for the transport of water and contaminants has been proven by a variety of authors using integral fieldtests as well as laboratory experiments ([2],[3],[4],[5],[6]) and analytical solutions ([7],[8],[9]). As about $50\,\%$ of the earth's surface [10] is covered by hard rocks integrated management of these resources largely depends on a thorough understanding of the aquifer's dynamical response to recharge and contamination.

Transport of water through the unsaturated zone is partially poorly unterstood due to the highly non-linear and intermittent flow processes involved ([11],[12],[13]). In unconsolidated media unsaturated flow is often simulated by volume-averaged effective modeling approaches such as the Richard's equation [14]. However, the behavior of water in unsaturated fractures is affected by a multitude of hydrodynamic effects that cannot be captured by classical continuum models and may give rise to highly nonlinear flow modes. Depending on the fracture properties (aperture, inclination, roughness) fluid flow within fracture elements is controlled by the interaction of body and surface forces. Thus gravity driven or capillary driven flow may prevail. Microscale modeling approaches should therefor be able to deal with the resulting highly dynamical interfaces and provide a flexible numerical tool for validation and prediction of transient flow. Furthermore transport relevant properties such as velocity and surface contact area are of interest for the characterization of matrix-fracture interaction and require adequate numerical techniques.

This paper demonstrates how Smoothed Particle Hydrodynamics (SPH) can be used to simulate small scale free-surface fluid flow in wide aperture fractures. Particular attention is paid to general approaches for calibration and verification of the SPH model for droplet flow.

II. Method

In the following we give a brief description of our model and the governing equations. More detailed derivations and approximations involved in the SPH method can be found for example in ([15],[16],[17]).

We use an SPH momentum conservation equation proposed in [15]:

$$\begin{aligned}\frac{d\mathbf{v}_i}{dt} = &-\sum_{j=1}^{N} m_j \left(\frac{P_j}{\rho_j^2} + \frac{P_i}{\rho_i^2} + \eta_{ij}\right) \boldsymbol{\nabla} W_i(|\mathbf{r}_i - \mathbf{r}_j|, h) \\ &+ \mathbf{g} + m_i \sum_{j=1}^{N} \mathbf{F_{ij}},\end{aligned} \tag{1}$$

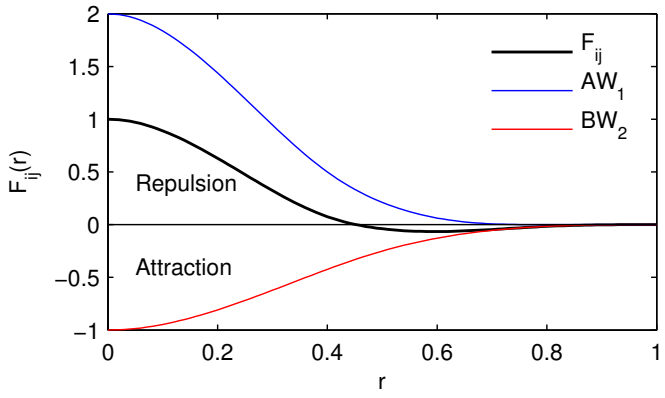

Fig. 1. Interaction potential

where $\mathbf{v}$ is the particle velocity, t is the time, P and ρ denote pressure and density, m is mass of particle i and $\mathbf{g}$ is the gravitational acceleration. We use a fourth-order weighting function W_i, [18]. For computational efficiency, the support of W is set to $h = 1.0$ and all particles are assumed to have the same mass, $m_i = 1.0$. All variables in the SPH model are given in consistent model units. The viscosity term η_{ij} is given by [19] as

$$\eta_{ij} = 2\mu \frac{\mathbf{v}_i - \mathbf{v}_j}{\rho_i \rho_j (\mathbf{r}_i - \mathbf{r}_j)^2} (\mathbf{r}_i - \mathbf{r}_j). \tag{2}$$

The surface tension is created by a particle-particle interaction forces $\sum_{j=1}^{N} \mathbf{F_{ij}}$, [15]. In this work we construct an interparticle force acting on particle i following [20] by superposition of two cubic spline kernels $W_1(|\mathbf{r}_i - \mathbf{r}_j|, h_1)$ and $W_2(|\mathbf{r}_i - \mathbf{r}_j|, h_2)$,

$$\mathbf{F_{ij}} = \begin{cases} s_{ij}[AW_1(r, h_1) + BW_2(r, h_2)] & |\mathbf{r}_i - \mathbf{r}_j| \leq h \\ 0 & |\mathbf{r}_i - \mathbf{r}_j| > h, \end{cases} \tag{3}$$

where $A = 2.0$, $h_1 = 0.8$, $B = -1.0$ and $h_2 = 1.0$ with $W_1(|\mathbf{r}_i - \mathbf{r}_j| > 0.8, h_1) = 0$. The resulting function is smooth and continous with a short-range repulsive and a long-range attractive part as seen in Fig. 1. The parameter s_{ij} controls the interaction strength and has values s_{fs} (fluid-solid) and s_{ff} (fluid-fluid).

Density is obtained from the general field approximation given by

$$\rho_i = \sum_{j=1}^{N} m_j W(|\boldsymbol{r}_i - \boldsymbol{r}_j|, h) \tag{4}$$

and the equation system is closed by a van der Waals equation of state (EOS)

$$P = \frac{\rho \frac{k_b}{m} T}{1 - \rho \frac{b}{m}} - \frac{a}{m} \rho^2 \tag{5}$$

where k_b is the Boltzmann constant, T is the temperature and a and b are the van der Waals constants. Values for the constants are $k_b T = 1.6$, $a = 3.0$ and $b = 1/3$.

III. Model Calibration

Fundamental fluid properties are initially defined by determining the surface tension. Using Young-Laplace the surface tension can be obtained from droplets in zero gravity

$$\sigma = \frac{R}{2} \Delta P_0 \tag{6}$$

where R is the droplet radius and ΔP_0 is the pressure gradient. As the surrounding pressure is zero (the airphase is not discretized using particles) $\Delta P_0 = P_0$. However, as the EOS does not consider the additional pressure contribution due to the interaction forces the total pressure has to be obtained through the Virial theorem as shown by [15] and [21]:

$$P_0 = \frac{1}{2dV} \sum_i \sum_j r_{ij} f_{ij} = \frac{1}{8 r_{virial}^3} \sum_i \sum_j r_{ij} f_{ij} \tag{7}$$

where $d = 3$ in a three-dimensional system, $r_{virial} = R - 1$ and $f_{ij} = m_i d\mathbf{v_i}/dt$. At equilibrium conditions the contribution of viscous forces to f_{ij} is zero thus the resulting pressure P_0 is independent of the prescribed model viscosity. As shown in Fig. 2 pressure and surface tension are nearly constant. However, for smaller droplets with radius close to h, the numerical resolution becomes insufficient and we observe a slight deviation from the Young-Laplace law. Corrections such as CSPM [22] or a kernel normalization [23] can be used to reduce this error. In the following, all SPH simulations use an interaction force $s_{ff} = 0.05$ i.e. a surface tension of $\sigma = 0.25$.

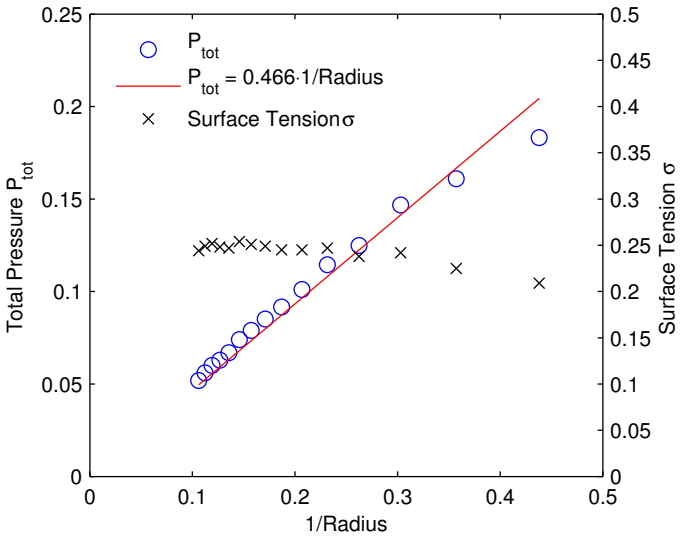

Fig. 2. Surface tension and pressure for various droplet sizes, $\mathbf{g} = 0$, $s_{ff} = 0.05$

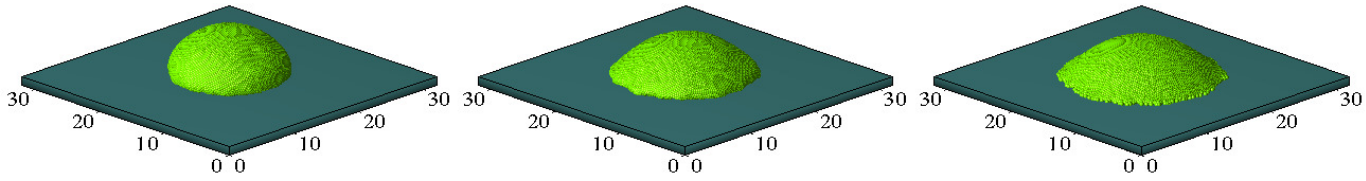

Fig. 3. Static contact angles for different fluid-solid interactions strengths. From left to right: $s_{fs} = 0.01, 0.03, 0.05$

A. Static Contact Angles

We use the Bond number and Eq. 6 to relate gravitational accelerations in the model units and the SI units:

$$Bo = (\frac{\rho g V^{2/3}}{\sigma})_{sph} = (\frac{\rho g V^{2/3}}{\sigma})_{SI}, \quad (8)$$

where $\rho = 999.7\,\mathrm{kg\,m^{-3}}$, $g = 9.81\,\mathrm{kg\,m\,s^{-2}}$ and $\sigma = 0.0742\,\mathrm{N\,m^{-1}}$ for water at average subsurface temperatures of 10 °C. The average density in the SPH simulations is $\rho = 39.2$.

The initially equilibrated droplet ($Bo = 1.0$) is slowly placed on the surface by gradually increasing the gravitational acceleration and the solid-fluid interaction force to their maximum values $\mathrm{g} = 0.0001790$ and $s_{sf} = 0.05$. The surface has a thickness of 4 h. The contact angle is measured when a stationary state is reached. The interaction force is then incrementally decreased ($s_{sf} = 0.05, 0.04, ...0.01, 0.005, 0.001$) to measure the dependence of the contact angle on s_{sf}.

Contact angles are measured visually for the shown simulations. We also fitted a polynomial to the particle hull yielding an analytical solution for the contact angle at the base of the droplet. Depending on the discretization this method may be less reliable as surfaces are not always perfectly smooth.

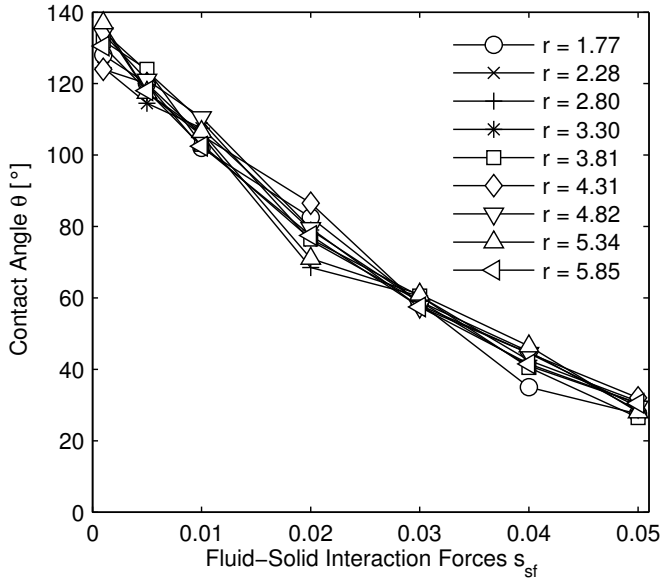

Fig. 4. Contact angles for varying interaction force s_{sf}. $Bo = 1.0$ for all radii.

In order to investigate the influence of discretization on the static contact angle we used different droplet radii while keeping the Bond number constant. As shown in Fig. 4 the highest contact angles of about $120° - 140°$ are measured for very low values $s_{sf} = 0.001$. Such high contact angles are likely for synthetic (super-)hydrophobic surfaces as often used in laboratory experiments. Water contact angles encountered on rock surfaces are much lower, ranging from $20° - 40°$ [9] which corresponds to values of s_{sf} between 0.05 and 0.04 where forces become comparable to the fluid-fluid interaction force s_{ff}. To study the effect of resolution several droplets with constant Bond number $Bo = 1.0$ but different radii ($R = 1.77$ h, 902 particles to $R = 5.85$ h, 77993 particles) were simulated. Simulations yielded contact angles within several percent of each other. Thus for stationary conditions the contact angle can be considered independent of the resolution. However, further studies are necessary for dynamic contact angle hysteresis under transient conditions as well as different Bond numbers.

IV. Transient Droplets

Experiments on droplet dynamics on surfaces have been investigated by numerous authors. In order to calibrate and verify our model we use a general scaling law as introduced by [24]. The proposed scaling relies on a simple force balance and states as follows:

$$Ca \sim Bo\ sin(\alpha) - \Delta_\theta \quad (9)$$

where the capillary number is defined as $Ca = \mu v/\sigma$, v is the droplet velocity, α is the surface inclination angle measured from the horizontal and Δ_θ is a perimeter-average projection factor of the surface tension. Following [9] we define a proportionality constant γ such that

$$Ca = \gamma\ Bo\ sin(\alpha) - \Delta_\theta \quad (10)$$

where γ and Δ_θ are empirical constants unique for a given fluid-solid system. As noted by [24] the linear scaling holds only for droplets with shapes close to a spherical cap. As soon as droplets begin to change their shape, e.g. develop

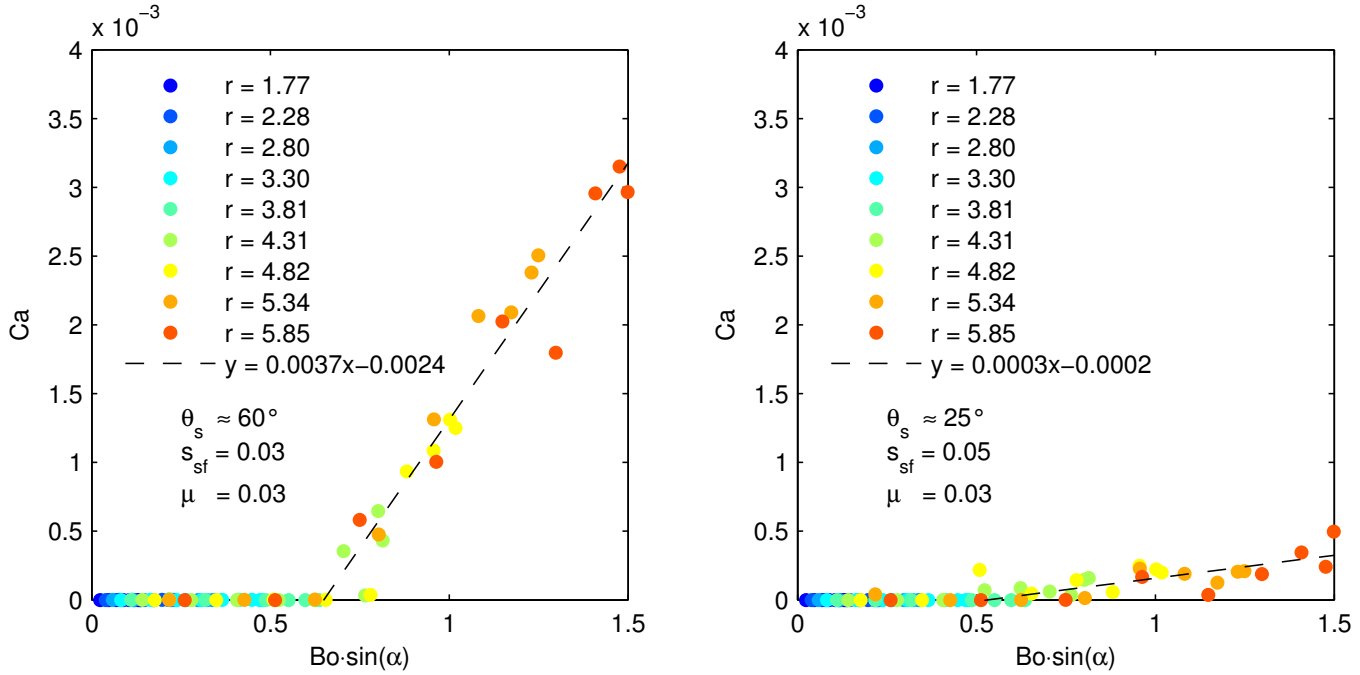

Fig. 5. Linear scaling for two different values of s_{sf}. Surface inclination angles are varied from 10° to 90°.

strong tails and possibly break up into smaller droplets the force balance assumptions fail such that droplets of different Bond numbers for a given fluid-solid system will not share common values γ and Δ_θ anymore.

The model domain for transient droplet flow simulations has sizes $x = 128\,\mathrm{h}$, $y = 64\,\mathrm{h}$ and $z = 16\,\mathrm{h}$ corresponding to $45.7 \times 22.8 \times 5.7$ mm. Droplets are initially placed on the surface close to $x = 0.0$. We then gradually increase the interaction force s_{sf} up to the maximum value (0.01, 0.02 ... 0.05) and wait until the droplet height remains constant. Gravitational acceleration is then slowly increased up to the maximum value of 0.0001139. The nine different droplets range from 0.14 to 1.5 in terms of the Bond number (droplet radii between 0.63 and 2.09 mm). The surface inclination ranges from 10° to 90° such that for every static contact angle θ_s 81 different values for $Bo\ sin(\alpha)$ are obtained. Droplet velocities are measured by tracking the droplet front position over time and evaluating dx/dt at maximum acceleration over a time intervall long enough to average out temporary fluctuations due to sudden particle movements at the droplet front. Such behavior mainly occurs at low Bond numbers close to the onset of droplet movement when body forces only partially exceed drag forces.

Fig. 5 shows two different simulation setups where $s_{sf} = 0.03$ and $s_{sf} = 0.05$ corresponding to static contact angles of 60° and 25°. Viscosity is $\mu = 0.03$ for all shown simulations. The results clearly show that within the given range of Bond numbers (i.e. droplets with radii smaller or in the order of the capillary length of water) the proposed scaling law holds. Topview droplet shapes are mostly round or become slightly cornered at higher Bond numbers (see Fig. 6). Note that for higher Bond numbers droplets may leave behind a thin film of fluid. In comparison to the total droplet volume and for the simulated timespan this net mass loss can be neglected. As no pearling or strong tailing effects can be observed, the simple force balance of [24] can be applied.

The values of γ and Δ_θ are close to values reported for example by [9]. However, as fractured rock surfaces are highly heterogeneous the exact value is not known and depends on the investigated rock properties. Reynolds numbers for such microscale systems can range from less than 5 to as much as 1100 with velocities of up to $70\,\mathrm{cm\,s^{-1}}$ as reported by [25] (laboratory experiments on broken glass surfaces) where

$$Re = \frac{\rho\ v\ V^{(1/3)}}{\mu}. \tag{11}$$

Maximum Reynolds numbers for simulations as shown in Fig. 5 are 302 ($\theta_s = 60°$) and 48 ($\theta_s = 25°$) with maximum velocities of $21\,\mathrm{cm\,s^{-1}}$ and $3.2\,\mathrm{cm\,s^{-1}}$. Further calibration of these characteristic parameters (e.g. as reported in laboratory experiments) can be achieved by simply adjusting the viscosity (assuming that static contact angles are known). However, given the relatively wide parameter ranges reported in literature and considering the data scarcity it should be of primary concern to provide physically correct model behavior as verified by the above dimensionless scaling law.

V. Conclusion

Application of the SPH method to hydrogeological modeling in unsaturated fractured aquifer systems enables us to gain

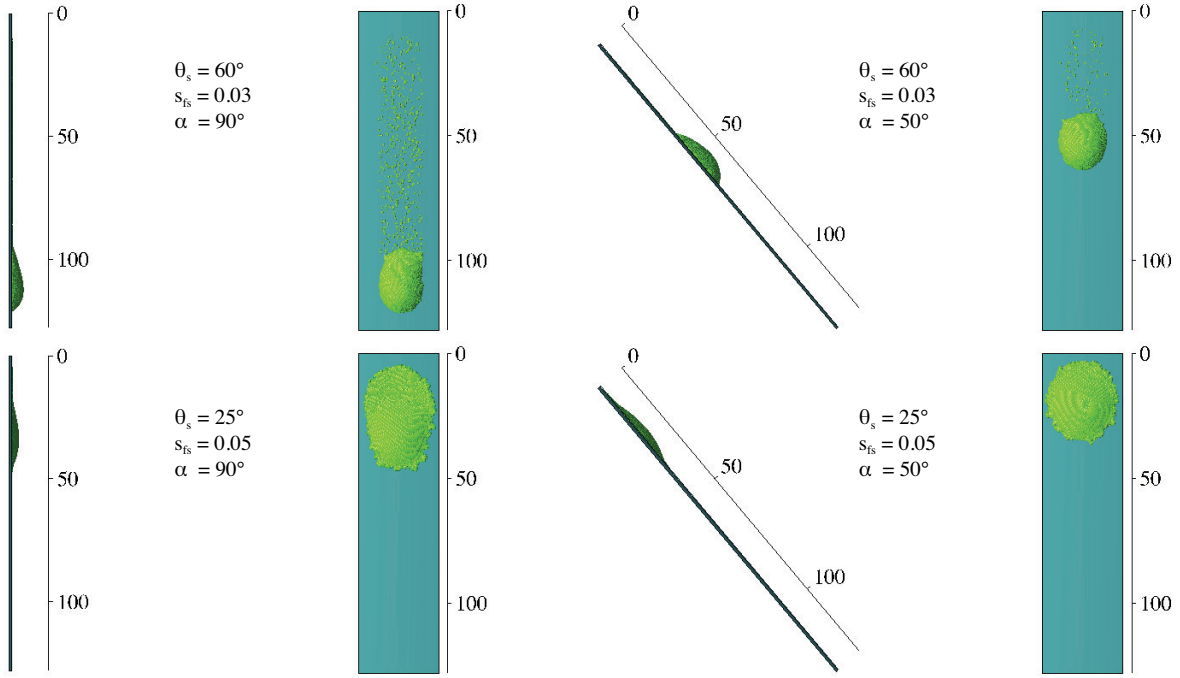

Fig. 6. Droplet ($R = 5.85$) for two different values of s_{sf} and two inclination angles at maximum velocity (same timestep shown in all pictures). Note that boundaries have a thickness of $4\,\mathrm{h}$ but are not shown here.

further insight into the highly nonlinear flow dynamics on such small scales. It is shown that the obtained static contact angles are independent of resolution, thus for stationary conditions a relatively coarse discretization may be used in order to save computation time. Furthermore we show that our model gives correct results for droplet flow according to the general scaling law proposed by [24]. Using dimensionless proportionality constants [9] we are able to define unique parameter combinations for a given fluid/solid system.

Due to the complex flow dynamics occurring on rough fracture surfaces further research is needed to verify additional flow regimes such as rivulet flow [26], (adsorbed) film flow ([27],[9],[2]) and corresponding regime transitions. Surface characteristics, in particular (micro-)roughness are currently not included for easier verification and comparison with available laboratory data. However, as shown by [28] the implementation of more complex geometries is possible and illustrates the flexibility of SPH.

ACKNOWLEDGMENT

This work was partially supported by the DAAD (German Academic Exchange Service) providing J. Kordilla with an international research scholarship at the Pacific Northwest National Laboratory (PNNL), USA. A. Tartakovsky was supported by the Laboratory Directed Research and Development program at PNNL. The Pacific Northwest National Laboratory is operated by Battelle for the U.S. Department of Energy under Contract DE-AC05-76RL01830.

REFERENCES

[1] M. Sauter, *Quantification and Forecasting of Regional Groundwater Flow and Transport in a Karst Aquifer (Gallusquelle, Malm, SW. Germany)*. Tübinger Geowissenschaftliche Arbeiten, 1992.

[2] T. K. Tokunaga, J. Wan, and S. R. Sutton, "Transient film flow on rough fracture surfaces" *Water Resources Research*, vol. 36, no. 7, pp. 1737–1746, 2000. [Online]. Available: http://www.agu.org/pubs/crossref/2000/2000WR900079.shtml

[3] G. W. Su, J. T. Geller, K. Pruess, and J. R. Hunt, "Solute transport along preferential flow paths in unsaturated fractures" *Water Resources Research*, vol. 37, no. 10, pp. 2481–2491, 2001. [Online]. Available: http://wwwrcamnl.wr.usgs.gov/uzf/abs_pubs/papers/WRR.37.10.pdf

[4] G. W. Su, J. T. Geller, J. R. Hunt, and K. Pruess, "Small-Scale Features of Gravity-Driven Flow in Unsaturated Fractures" *Vadose Zone Journal*, vol. 3, no. 2, pp. 592–601, May 2004. [Online]. Available: http://vzj.scijournals.org/cgi/doi/10.2113/3.2.592

[5] M. J. Nicholl, R. J. Glass, and S. W. Wheatcraft, "Gravity-driven infiltration instability in initially dry nonhorizontal fractures" *Water Resources Research*, vol. 30, no. 9, pp. 2533–2546, 1994. [Online]. Available: http://www.agu.org/pubs/crossref/1994/94WR00164.shtml

[6] M. J. Nicholl and R. J. Glass, "Infiltration into an Analog Fracture" *Vadose Zone Journal*, vol. 4, no. 4, p. 1123, 2005. [Online]. Available: https://www.soils.org/publications/vzj/abstracts/4/4/1123

[7] T. A. Ghezzehei, "Flow diversion around cavities in fractured media" *Water Resources Research*, vol. 41, pp. 1–5, 2005.

[8] D. Or and T. A. Ghezzehei, "Traveling liquid bridges in unsaturated fractured porous media" *Transport in Porous Media*, vol. 68, no. 1, pp. 129–151, Nov. 2006. [Online]. Available: http://www.springerlink.com/index/10.1007/s11242-006-9060-9

[9] T. A. Ghezzehei, "Constraints for flow regimes on smooth fracture surfaces" *Water Resources Research*, vol. 40, pp. 1 – 14, 2004.

[10] B. B. Singhal and R. P. Gupta, *Applied Hydrogeology of Fractured Rocks*. Springer, 2010.

[11] T. A. Ghezzehei and D. Or, "Liquid fragmentation and intermittent flow regimes in unsaturated fractured media" *Water Resources Research*, vol. 41, no. 12, pp. 1–10, 2005. [Online]. Available: http://www.agu.org/pubs/crossref/2005/2004WR003834.shtml

[12] D. Or and M. Tuller, "Flow in unsaturated fractured porous media: Hydraulic conductivity of rough surfaces" *Water Resources Research*, vol. 36, no. 5, pp. 1165–1177, 2000.

[13] M. I. Dragila and N. Weisbrod, "Parameters affecting maximum fluid transport in large aperture fractures" *Advances in Water Resources*, vol. 26, pp. 1219–1228, 2003.

[14] L. A. Richards, "Capillary Conduction of Liquids Through Porous Mediums" *Physics*, vol. 1, no. 5, p. 318, 1931. [Online]. Available: http://link.aip.org/link/JAPIAU/v1/i5/p318/s1&Agg=doi

[15] A. M. Tartakovsky and P. Meakin, "Modeling of surface tension and contact angles with smoothed particle hydrodynamics" *Physical Review E*, vol. 72, pp. 1–9, 2005.

[16] J. Monaghan, "Why particle methods work," *Journal on Scientific and Statistical Computing*, vol. 3, no. 4, pp. 422 – 433, 1982.

[17] M. B. Liu and G. R. Liu, "Smoothed Particle Hydrodynamics (SPH): an Overview and Recent Developments" *Archives of Computational Methods in Engineering*, vol. 17, no. 1, pp. 25–76, 2010. [Online]. Available: http://www.springerlink.com/index/10.1007/s11831-010-9040-7

[18] A. M. Tartakovsky and P. Meakin, "A smoothed particle hydrodynamics model for miscible flow in three-dimensional fractures and the two-dimensional Rayleigh–Taylor instability" *Journal of Computational Physics*, vol. 207, pp. 610–624, 2005.

[19] J. Morris, "Modeling Low Reynolds Number Incompressible Flows Using SPH" *Journal of Computational Physics*, vol. 136, no. 1, pp. 214–226, Sep. 1997. [Online]. Available: http://linkinghub.elsevier.com/retrieve/pii/S0021999197957764

[20] M. Liu, P. Meakin, and H. Huang, "Dissipative particle dynamics with attractive and repulsive particle-particle interactions" *Physics of Fluids*, vol. 18, no. 1, p. 017101, 2006. [Online]. Available: http://link.aip.org/link/PHFLE6/v18/i1/p017101/s1&Agg=doi

[21] M. Allen and D. Tildesley, *Computer Simulation of Liquids*. Clarendon Press, Oxford, 1989.

[22] J. Chen, J. Beraun, and T. Carney, "A corrective smoothed particle method for boundary value problems in heat conduction" *International Journal for Numerical Methods in Engineering*, vol. 46, no. 2, pp. 231–252, 1999. [Online]. Available: http://onlinelibrary.wiley.com/doi/10.1002/(SICI)1097-0207(19990920)46:2<231::AID-NME672>3.0.CO;2-K/abstract

[23] P. Randles, "Smoothed Particle Hydrodynamics: Some recent improvements and applications" *Computer Methods in Applied Mechanics and Engineering*, vol. 139, no. 1-4, pp. 375–408, Dec. 1996. [Online]. Available: http://linkinghub.elsevier.com/retrieve/pii/S0045782596010900

[24] T. Podgorski, J.-M. Flesselles, and L. Limat, "Corners, Cusps, and Pearls in Running Drops" *Physical Review Letters*, vol. 87, no. 3, pp. 1–4, Jun. 2001. [Online]. Available: http://link.aps.org/doi/10.1103/PhysRevLett.87.036102

[25] M. I. Dragila, N. Weisbrod, and N. R. Council, "Fluid motion through an unsaturated fracture junction" *Water Resources Research*, vol. 40, pp. 1–11, 2004.

[26] M. I. Dragila and N. Weisbrod, "Flow in Menisci Corners of Capillary Rivulets" *Vadose Zone Journal*, vol. 3, pp. 1439–1442, 2004.

[27] M. Tuller and D. Or, "Hydraulic conductivity of variably saturated porous media : Film and corner flow in angular pore space" *Water Resources Research*, vol. 37, no. 5, pp. 1257 – 1276, 2001.

[28] A. M. Tartakovsky and P. Meakin, "Simulation of Unsaturated Flow in Complex Fractures Using Smoothed Particle Hydrodynamics" *Vadose Zone Journal*, vol. 4, no. 3, pp. 848–855, 2005. [Online]. Available: http://vzj.scijournals.org/cgi/doi/10.2136/vzj2004.0178